Bulk-edge correspondence in open photonic systems

Tetsuyuki Ochiai

Research Center for Functional Materials, National Institute for Materials Science, Tsukuba 305-0044, Japan

ARTICLE HISTORY
Compiled August 26, 2020

ABSTRACT
We study the bulk-edge correspondence in topological photonic crystals with open boundary. If boundary is open, edge states become leaky inside the light cone, but still exhibit a chiral and gapless property taking into account the blurring of their band structure due to the leakage. The so-called bulk-edge correspondence is thus verified. On the other hand, in closed boundaries, edge states exhibit the well-defined band structure without the blurring and show clearly the bulk-edge correspondence. To demonstrate these results, we employ the transfer-matrix formalism and derive reflection matrices of semi-infinite systems. Optical density of states for the system with open boundaries is available via the Krein-Friedel-Lloyd formula for the reflection matrices. The leaky photonic band structure of the edge states is obtained by following the peaks and widths of the density of states as a function of momentum parallel to the boundary. Our derivation of the leaky band structure does not rely on possible effective non-hermitian hamiltonians, but relies on a first-principles calculation of the Maxwell equation.

KEYWORDS
topological photonics; edge states; density of states; open quantum systems

1. Introduction

Radiation fields are real-valued. This implies that their frequencies are positive-definite, regardless of their spatial profiles, localized or extended. The "work function" for photons is completely absent between a photonic medium [such as photonic crystal (PhC)] and outer medium (such as air). In this sense, any photonic systems are open to the outer medium, and inversely, an incoming wave in the outer medium can excite internal modes in a photonic system, regardless of frequency, This "open"ness of photonic systems shows a striking contrast to that in electronic systems, where internal modes are protected from the mixing with outer modes by finite work functions. The "open"ness of the electronic systems is restricted, only through other kinds of excitation modes such as phonons.

Suppose that there is a topologically nontrivial photonic system [1,2] with boundary. We expect that the system has gapless boundary states, in accordance with the so-called bulk-edge correspondence [3]. However, such a boundary state is embedded in the radiation continuum of the outer medium, so that the state becomes leaky unless it is outside the light cone. We considered this situation in [4], and found the bulk-edge correspondence certainly works provided that the blurring (in frequency) of the leaky

boundary states is taken into account.

Here, we revisit this problem in a more ideal situation than in [4] and show clearly that the bulk-edge correspondence certainly holds. In this demonstration, the transfer-matrix formalism plays a crucial role. It enables us to study the photonic band structures in the bulk, reflection matrices of semi-infinite systems, skin depth at the surface, and so on [5,6]. The reflection matrix together with a boundary condition determines the dispersion relation of possible boundary states, via the Krein-Friedel-Lloyd formula [7–9], as we show in this paper.

Recently, many important discoveries have been made in non-hermitian [10] and/or PT symmetric [11], and/or open quantum systems [12]. The discoveries include periodic tables in topological phases [13], non-hermitian skin effect [14], interaction effects [15]. This paper is closely related to several issues in open quantum systems. However, in studying such a system, possible issues relevant to the light cone are completely absent. The light cone is inherent in photonic systems and gives severe constraints on them. For instance, the light cone separates the momentum space into two distinct regions, inside and outside the light cone. Inside the light cone, photons can leak to outer space, whereas outside the light cone, photons are totally internal reflected. The Brillouin-zone folding in PhCs further complexifies the momentum space. Such a complexity is usually not taken into account in the study of open quantum systems. Therefore, the issues on the light cone may give some insights to open quantum systems.

This paper is organized as follows. In Sec. 2, we present a theoretical framework to investigate PhCs with open boundaries. In Sec. 3, we focus on typical topological PhCs via the time-reversal-symmetry breaking, and verify the bulk-edge correspondence. Section 4 is devoted to present non-topological PhCs with the time reversal symmetry and show that the edge states are clearly gapped. Finally, in Sec. 5, we summarize the results obtained in this paper.

2. Bulk and edge by transfer-matrix formalism

In what follows, we assume two-dimensional (2D) PhCs with the transnational invariance in the z direction, and consider the in-plane propagation of light ($k_z = 0$). The light polarization is decoupled into the transverse-electric (TE) polarization characterized by nonzero E_x, E_y, and H_z and the transverse-magnetic (TM) polarization characterized by nonzero E_z, H_x, and H_y. Here, we assume the TM polarization. The extension of the following formalism to the TE polarization is straight-forward.

Suppose that the bulk PhC is made of a periodic stack of identical monolayers with relative shift $\boldsymbol{s}$ between two adjacent layers, as depicted in Fig. 1.

[Figure 1 about here.]

The monolayer consists of circular rods with lattice constant d in the x direction. The dielectric constant of the background medium is denoted as ϵ_b. The stacking direction is taken to be y direction. In the n-th void region between the n-th layer and $n+1$-th

layer, the electric field is expressed as

$$E_z^{(n)}(\boldsymbol{x}) = \sum_h (a_h^{+(n)} \mathrm{e}^{\mathrm{i}\boldsymbol{K}_h^+ \cdot (\boldsymbol{x}-\boldsymbol{x}_n)} + a_h^{-(n)} \mathrm{e}^{\mathrm{i}\boldsymbol{K}_h^- \cdot (\boldsymbol{x}-\boldsymbol{x}_n)}), \tag{1}$$

$$\boldsymbol{K}_h^{\pm} = (k_x + h)\hat{x} \pm \gamma_h \hat{y}, \quad \gamma_h = \sqrt{q_b^2 - (k_x + h)^2}, \tag{2}$$

$$h = \frac{2\pi \boldsymbol{Z}}{d}, \quad q_b = \frac{\omega}{c}\sqrt{\epsilon_b}. \tag{3}$$

Here, $\boldsymbol{x}_n$ is the reference point of the n-th void region, satisfying $\boldsymbol{x}_{n+1} - \boldsymbol{x}_n = \boldsymbol{s}$, k_x is the Bloch momentum, and ω is the angular frequency of the radiation field concerned. The monolayer S-matrix gives the relation among the plane-wave-expansion (PWE) coefficients $a_h^{\pm}$ of two successive void regions as

$$\begin{pmatrix} a_h^{+(n+1)} \\ a_h^{-(n)} \end{pmatrix} = \sum_{h'} \begin{pmatrix} S_{hh'}^{++} & S_{hh'}^{+-} \\ S_{hh'}^{-+} & S_{hh'}^{--} \end{pmatrix} \begin{pmatrix} a_{h'}^{+(n)} \\ a_{h'}^{-(n+1)} \end{pmatrix}. \tag{4}$$

In a short-hand notation, we rewrite it as

$$\begin{pmatrix} \boldsymbol{a}^{+(n+1)} \\ \boldsymbol{a}^{-(n)} \end{pmatrix} = S(\omega, k_x) \begin{pmatrix} \boldsymbol{a}^{+(n)} \\ \boldsymbol{a}^{-(n+1)} \end{pmatrix}, \tag{5}$$

$$S(\omega, k_x) = \begin{pmatrix} S^{++} & S^{+-} \\ S^{-+} & S^{--} \end{pmatrix}. \tag{6}$$

The S-matrix is numerically available by the 2D version of the layer Korringa-Kohn-Rostoker method [16–18]. The S-matrix of consecutive two monolayers (S_2) is obtained by the layer-doubling procedure as [19]

$$\begin{pmatrix} a_h^{+(n+2)} \\ a_h^{-(n)} \end{pmatrix} = \sum_{h'} \begin{pmatrix} (S_2)_{hh'}^{++} & (S_2)_{hh'}^{+-} \\ (S_2)_{hh'}^{-+} & (S_2)_{hh'}^{--} \end{pmatrix} \begin{pmatrix} a_{h'}^{+(n)} \\ a_{h'}^{-(n+2)} \end{pmatrix}, \tag{7}$$

$$S_2^{++} = S^{++}(1 - S^{+-}S^{-+})^{-1}S^{++}, \tag{8}$$

$$S_2^{+-} = S^{+-} + S^{++}S^{+-}(1 - S^{-+}S^{+-})^{-1}S^{--}, \tag{9}$$

$$S_2^{-+} = S^{-+} + S^{--}S^{-+}(1 - S^{+-}S^{-+})^{-1}S^{++}, \tag{10}$$

$$S_2^{--} = S^{--}(1 - S^{-+}S^{+-})^{-1}S^{--}, \tag{11}$$

$$\tag{12}$$

The successive application of the layer doubling produces the S-matrix of 2^m (m: positive integer) layers, and the transmittance and reflectance of the 2^m-layer-thick PhC are obtained.

The band structure of the corresponding bulk PhC is obtained from the monolayer S-matrix. Between two adjacent voids, the Bloch theorem reads

$$E_z^{(n+1)}(\boldsymbol{x} + \boldsymbol{s}) = \mathrm{e}^{\mathrm{i}\boldsymbol{k}\cdot\boldsymbol{s}} E_z^{(n)}(\boldsymbol{x}), \tag{13}$$

where $\boldsymbol{x}$ is assumed to be in the n-th void. The lattice vectors of the bulk PhC are spanned by $\boldsymbol{e}_1 = d\hat{x}$ and $\boldsymbol{e}_2 = \boldsymbol{s}$. On the other hand, $a_h^{\pm(n+1)}$ are related to $a_h^{\pm(n)}$ via

the monolayer S-matrix. Therefore, the Bloch theorem reduces to the diagonalization of the transfer matrix as

$$T(\omega, k_x) \begin{pmatrix} \boldsymbol{a}^{+(n)} \\ \boldsymbol{a}^{-(n)} \end{pmatrix} = \mathrm{e}^{\mathrm{i}\boldsymbol{k}\cdot\boldsymbol{s}} \begin{pmatrix} \boldsymbol{a}^{+(n)} \\ \boldsymbol{a}^{-(n)} \end{pmatrix}, \tag{14}$$

$$\begin{pmatrix} \boldsymbol{a}^{+(n+1)} \\ \boldsymbol{a}^{-(n+1)} \end{pmatrix} = T(\omega, k_x) \begin{pmatrix} \boldsymbol{a}^{+(n)} \\ \boldsymbol{a}^{-(n)} \end{pmatrix}, \tag{15}$$

$$T(\omega, k_x) = \begin{pmatrix} S^{++} - S^{+-}(S^{--})^{-1}S^{-+} & S^{+-}(S^{--})^{-1} \\ -(S^{--})^{-1}S^{-+} & (S^{--})^{-1} \end{pmatrix} \tag{16}$$

This is an *on-shell* band calculation; the momentum in the $\boldsymbol{s}$ direction is obtained as the outputs, while the frequency and momentum in the x direction are given as the inputs. The transfer matrix T is not unitary, so that the eigen-momenta $\boldsymbol{k}\cdot\boldsymbol{s}$ are not limited in real value. Among them, the real-valued ones are propagating eigenmodes that correspond to the photonic band modes in an ordinary (*off-shell*) band calculation. The complex-valued ones are evanescent eigenmodes which are hidden in the ordinary band calculation. In a bulk band gap, no propagating eigenmodes are found. The evanescent eigenmodes having the smallest absolute imaginary part in $\boldsymbol{k}\cdot\boldsymbol{s}$ determine the penetration depth of the incident wave in the band gap.

The transfer matrix is also very important in determining possible surface states in the PhC. The diagonalization of the transfer matrix leads to

$$T = V\Lambda V^{-1}, \tag{17}$$

$$\Lambda = \mathrm{diag}(\mathrm{e}^{\mathrm{i}\boldsymbol{k}\cdot\boldsymbol{s}}) = (\Lambda_+, \Lambda_-), \tag{18}$$

$$V = \begin{pmatrix} A & B \\ C & D \end{pmatrix}, \quad V^{-1} = \begin{pmatrix} A' & B' \\ C' & D' \end{pmatrix}, \tag{19}$$

Within a bulk band gap, the eigenvalues are either forward evanescent or backward evanescent. Here, $\Lambda_{+(-)}$ represents the forward (backward) evanescent eigenmodes. We note that the transfer matrix of the N-layer system is simply T^N and that $\Lambda_+^N \to 0$ as $N \to \infty$. By transforming back to the S-matrix via Eq. (16), the S-matrix of infinitely thick PhC becomes

$$S_\infty = \begin{pmatrix} 0 & R' \\ R & 0 \end{pmatrix}. \tag{20}$$

Here, R is the reflection matrix of the semi-infinite system for an incident wave from the bottom, and is given by

$$R = CA^{-1} = -D'^{-1}C' \tag{21}$$

Similarly, the reflection matrix R' for an incident wave from the top is given by

$$R' = BD^{-1} = -A'^{-1}B'. \tag{22}$$

By truncating into open diffraction channels, these reflection matrices are shown to

be unitary as

$$\tilde{R}^\dagger \tilde{R} = 1, \tag{23}$$

$$\tilde{R}_{h_\mathrm{o} h'_\mathrm{o}} = \sqrt{\gamma_{h_\mathrm{o}}} R_{h_\mathrm{o} h'_\mathrm{o}} \frac{1}{\sqrt{\gamma_{h'_\mathrm{o}}}}, \tag{24}$$

where h_o represents an open diffraction channel.

From the reflection matrix, we can calculate the eigenfrequency spectrum of possible surface states. Inside the light cone, the eigenfrequencies become complex owing to the leakage to the outer space. They have imaginary parts representing the radiation loss. A conventional way to calculate such energy spectra is to diagonalizing effective (and often non-well-defined) non-hermitian hamiltonians that include the loss. However, we do not employ such a scheme. Instead, we consider the well-defined transfer matrix and extract the information of the complex energy spectrum from it.

The key quantity is the density of states (DOS) of photons. Let us count the number of possible radiation modes by imposing the Dirichlet boundary condition at far fields. Far away the boundary surface of the PhC, we put the perfect-electric-conductor (PEC) wall parallel to the boundary. The boundary condition is simply given by

$$E_z(x, -L) = 0, \tag{25}$$

where we put the PEC wall at $y = -L$. Then, we have

$$a^{+(0)}_{h_\mathrm{o}} \mathrm{e}^{-\mathrm{i}\gamma_{h_\mathrm{o}} L} + a^{-(0)}_{h_\mathrm{o}} \mathrm{e}^{\mathrm{i}\gamma_{h_\mathrm{o}} L} = 0, \tag{26}$$

where we assume $\boldsymbol{x}^{(0)} = 0$. Here, we drop unphysical evanescent waves that are exponentially growing as $y \to -\infty$. Then, we obtain

$$\sum_{h'_\mathrm{o}} \left(\mathrm{e}^{-2\mathrm{i}\gamma_{h_\mathrm{o}} L} \delta_{h_\mathrm{o} h'_\mathrm{o}} + R_{h_\mathrm{o} h'_\mathrm{o}} \right) a^{+(0)}_{h'_\mathrm{o}} = 0, \tag{27}$$

in a bulk band gap. Let us consider the case that there is only one open channel. In this case, the reflection coefficient $R_{h_\mathrm{o} h_\mathrm{o}}$ is just a phase factor. Then we have

$$2\gamma_{h_\mathrm{o}} L + \arg(R_{h_\mathrm{o} h_\mathrm{o}}) = (2m+1)\pi \quad (m \in \boldsymbol{Z}). \tag{28}$$

The optical DOS per unit angular frequency is then given by

$$\rho = \frac{\Delta m}{\Delta \omega} = \frac{1}{\pi} \frac{\partial \gamma_{h_\mathrm{o}}}{\partial \omega} L + \frac{1}{2\pi} \frac{\partial}{\partial \omega} \arg(R_{h_\mathrm{o} h_\mathrm{o}}). \tag{29}$$

The first term in the right hand side is the DOS in free space with length L, and the second term is the contribution of the semi-infinite PhC. Therefore, the increment of the DOS due to the semi-infinite PhC structure is

$$\Delta\rho(\omega, k_x) = \frac{1}{2\pi} \frac{\partial}{\partial \omega} \arg(R_{h_\mathrm{o} h_\mathrm{o}}). \tag{30}$$

Here, $\arg(R_{h_\mathrm{o} h_\mathrm{p}})$ is nothing but the scattering phase shift. Therefore, the above equation is the optical analogue of the Krein-Friedel-LLoyd formula, or in other words, the

differential form of the Friedel sum rule [20]. If there are more than one open channels, the above expression is generalized as [21]

$$\Delta\rho(\omega, k_x) = \frac{1}{2\pi}\frac{\partial}{\partial\omega}\arg(\det\tilde{R}). \tag{31}$$

By following the peak frequency ω_c of the DOS as a function of k_x, we obtain the band structure of the leaky surface states.

Outside the light cone, there is no open channel. Therefore, the surface states cannot leak to the outer region. These true guided modes are determined as

$$\det B' = 0. \tag{32}$$

This completes the band calculation of the surface states in open photonic systems.

In a closed boundary capped by the PEC wall, the boundary condition is the same as Eq. (25). However, we have to take account of all the diffraction channels as

$$\sum_{h'} \left(\mathrm{e}^{-2\mathrm{i}\gamma_h L}\delta_{hh'} + R_{hh'}\right) a_{h'}^{+(0)} = 0. \tag{33}$$

If the system is covered by the perfect-magnetic-conductor (PMC) wall, the boundary condition is changed as

$$H_x(x, -L) = 0. \tag{34}$$

The secular equation for the surface states is given by

$$\sum_{h'} \left(\mathrm{e}^{-2\mathrm{i}\gamma_h L}\delta_{hh'} - R_{hh'}\right) a_{h'}^{+(0)} = 0. \tag{35}$$

In the previous study of Ref. [4], the authors considered the optical DOS for finite-thick PhC with lower and upper open boundaries. Therefore, the contribution of the lower and upper surface states to the DOS is mixed. It is quite often the case that the two peaks of the DOS merge to a single peak, so that we cannot separate each contribution. Using the semi-infinite system as we do in this paper, we can separate each contribution. Then, we can verify possible bulk-edge correspondence rule.

3. Topological photonic crystal without time-reversal symmetry

Let us first consider a typical topological PhC with a magneto-optical medium. In the magneto-optical medium, the permeability tensor in plane is given by

$$\overleftrightarrow{\mu} = \begin{pmatrix} \mu & \mathrm{i}\kappa \\ -\mathrm{i}\kappa & \mu \end{pmatrix}, \tag{36}$$

assuming the applied magnetic field (or spontaneous magnetization) along the z direction. The parameter κ represents the degree of the magneto-optical effect and a nonzero κ breaks the time-reversal symmetry. Suppose that the PhC consists of the honeycomb array of circular cylinders with the magneto-optical effect. Figure 2 shows the photonic band structures of the PhCs.

[Figure 2 about here.]

The photonic band structure without the magneto-optical effect exhibits the Dirac cones at the Brillouin zone corners provided that the two sites of the honeycomb lattice are equivalent. If the magneto-optical effect is introduced in the cylinder, or if the inversion-symmetry breaking is introduced by a difference between the A and B sites of the honeycomb lattice, the photonic band gap opens around the Dirac cones. In the former case, the relevant photonic bands become topological having the Chern numbers of ± 1. In the latter case, however, the photonic bands are topologically trivial with vanishing Chern number.

Figure 3 shows the photonic band structure of the zigzag and armchair edge states for the PEC or PMC boundary. Both the upper and lower edges of the semi-infinite PhC are considered.

[Figure 3 about here.]

In all the cases, the edge states are clearly gapless; their dispersion curve traverses the bulk band gap.

In the zigzag edges, the band structures are quite similar to those of the domain-wall fermion [22]. Namely, the almost linear dispersion is observed in the K and K' valleys. The edge states emerge in the opposite valley with the same chirality between the PEC and PMC boundary. Here, we refer to the chiality as the sign of the average group velocity of the edge states. The chirality is opposite between the upper and lower edges. Such a selective emergence of the chiral edge states are also obtained in the domain wall introduced in the PhCs [23].

The almost-linear dispersion can be understood as follows. Around the K and K' valleys, the $\boldsymbol{k}\cdot\boldsymbol{p}$ effective Hamiltonian is given by [24],

$$\mathcal{H}_{\mathrm{K}} = v(\sigma_3\delta k_x - \sigma_1\delta k_y) + \sigma_2 M, \tag{37}$$

$$\mathcal{H}_{\mathrm{K}'} = -v(\sigma_3\delta k_x - \sigma_1\delta k_y) + \sigma_2 M, \tag{38}$$

$$E_z(\boldsymbol{x}) = c_1 E_z^{(1)}(\boldsymbol{x}) + c_2 E_z^{(2)}(\boldsymbol{x}). \tag{39}$$

Here, σ_i $(i = 1, 2, 3)$ is the Pauli matrix, $\delta\boldsymbol{k}$ is the deviation of the momentum from the K or K' point, and M is the Dirac mass proportional to κ. The Hamiltonian acts on the phase space spanned by c_1 and c_2. The base functions $E_z^{(1)}$ and $E_z^{(2)}$ are the doubly degenerate eigenfunctions of the unperturbed honeycomb-lattice system at K or K'. That is, the modes at the Dirac point of Fig. 2. They form the E representation of C_{3v}, which is the $\boldsymbol{k}$ group at K or K' of the unperturbed system. We assume that $E_z^{(1)}$ has the even parity with respect to the mirror plane relevant to the K and K' points, and that $E_z^{(2)}$ has the odd parity, because the E representation behaves as (x, y). Therefore, $E_z^{(2)} = 0$ on the mirror plane.

To study possible edge states within the effective hamiltonian, we replace δk_y by momentum operator $-\mathrm{i}\partial/\partial y$. Then, we have the following eigenvalue equation:

$$\mathcal{H}\left(\delta k_x, -\mathrm{i}\frac{\partial}{\partial y}\right)\begin{pmatrix} c_1 \\ c_2 \end{pmatrix} = \mathcal{E}\begin{pmatrix} c_1 \\ c_2 \end{pmatrix}. \tag{40}$$

We can easily show that the equation around the K point has the edge-state solution

of

$$\mathcal{E} = -v\delta k_x, \quad c_1 = 0, \quad c_2 \propto \mathrm{e}^{\mathrm{i}\delta k_x x + \frac{M}{v} y}, \tag{41}$$

provided that 1) the PEC boundary is imposed on the mirror plane and 2) $\exp((M/v)y)$ is decaying away from the boundary. The second condition implies that if $M/v > 0$, then the upper edge states are allowed to exist. Otherwise, if $M/v < 0$, the lower edge states are allowed. Similarly, the following solution is also available around the K' point:

$$\mathcal{E} = v\delta k_x, \quad c_1 = 0, \quad c_2 \propto \mathrm{e}^{\mathrm{i}\delta k_x x - \frac{M}{v} y}, \tag{42}$$

provided that 1) the PEC boundary is imposed on the mirror plane and 2) $\exp(-(M/v)y)$ is decaying away from the boundary.

As for the PMC boundary, possible solutions are

$$\mathcal{E} = v\delta k_x, \quad c_1 \propto \mathrm{e}^{\mathrm{i}\delta k_x x - \frac{M}{v} y}, \quad c_2 = 0, \tag{43}$$

around K only for decaying $\exp(-(M/v)y)$, and

$$\mathcal{E} = -v\delta k_x, \quad c_1 \propto \mathrm{e}^{\mathrm{i}\delta k_x x + \frac{M}{v} y}, \quad c_2 = 0, \tag{44}$$

around K' only for decaying $\exp((M/v)y)$.

These four solutions correspond to the four dispersion curves in Fig. 3 (a). The emergence of the edge states are fully consistent with $v > 0$ and $M < 0$, as can be numerically checked from the unperturbed wave functions in the $\boldsymbol{k} \cdot \boldsymbol{p}$ perturbation.

In the armchair edge, the dispersion curve is not so simple, and is extended in the entire surface Brillouin zone. The description by the $\boldsymbol{k} \cdot \boldsymbol{p}$ effective hamiltonian is not efficient, because the hamiltonian is only valid around the K and K' valleys. The edge states still exhibit the chiral and gapless property, namely, the dispersion curve traverses the band gap with positive average slope for the upper edge and negative average slope for the lower edge. The complexity of the dispersion curve partially comes from the fact that the two Dirac cones at K and K' are overlaid after the projection to the surface Brillouin zone.

In the boundary capped by the PEC or PMC wall, the edge states are well-defined as shown in Fig. 3. They have pure real eigenfrequencies regardless of momentum. In the open boundary, however, the band structure is blurred, as they have nonzero imaginary part in their eigenfrequencies.

Figure 4 shows the photonic band structure of the edge states in the open boundary. The imaginary parts are also plotted as the error bars.

[Figure 4 about here.]

In the zigzag case, the edge states emerge outside the light cone, so that the band structure is well-defined. It exhibits the chiral and gapless property. In the armchair case, the band structure emerges both inside and outside the light cone. The center of the error bar represents the resonant frequency of the edge states, showing the chiral and gapless property. The heights of the error bar represent the inverse lifetimes, which decrease toward the light line $\omega = c|k_\parallel|$, and vanishes on it.

Figure 5 shows the increment of the DOS at $k_\parallel d_{\mathrm{arm}}/2\pi = 0.25$.

[Figure 5 about here.]

By a Lorentzian fit of the DOS via

$$\Delta\rho(\omega, k_x) = \frac{\frac{\Gamma}{\pi}}{(\omega - \omega_c) + \Gamma^2}, \quad Q = \frac{\omega_c}{2\Gamma}, \tag{45}$$

we obtain quality factor $Q = 46$ for the lower edge state, and $Q = 34$ for the upper edge state. In the actual calculation of the quality factor, we employ a numerical fitting of the phase shift by the Breit-Wigner formula:

$$\det\tilde{R} = \mathrm{e}^{2\mathrm{i}\delta_0}\frac{\omega - \omega_0 - \mathrm{i}\Gamma}{\omega - \omega_0 + \mathrm{i}\Gamma}, \tag{46}$$

from which the Lorentzian form of the DOS is derived.

In the PEC/PMC boundary case, the distance between the PhC edge and PEC/PMC wall is crucial. In Fig. 3, we put the PEC/PMC wall at the mirror plane (zigzag edge) or glide plane (armchair edge) of the bulk PhC. In the former case, the simple analytic solutions of Eqs. (41-44) are available, and describe the numerical solutions fairly well. However, if the PEC/PMC wall is put off the mirror/glide plane, such an analytic solution is not available. By increasing the distance L between the PhC edge and PEC/PMC wall, the photonic band structure approaches to that in the open boundary, while keeping the chiral and gapless property, as shown in Fig. 6.

[Figure 6 about here.]

Even at $L = a/2$, the dispersion relation is nearly equal to that in the open boundary. Thus, we can estimate the edge-state dispersion in the open boundary by increasing distance L.

4. Nontopological photonic crystal without space-inversion symmetry

For comparison, we consider a nontopological PhC without the magneto-optical effect. The time-reversal symmetry thus holds and the Chern number vanishes. We consider the honeycomb-lattice PhC with a difference in the dielectric constants between A and B rods, yielding the space-inversion-symmetry breaking and the band gap at the Dirac points. The effective Hamiltonian around K and K' are now given by [24]

$$\mathcal{H}_K = v(\sigma_3\delta k_x - \sigma_1\delta k_y) + M\sigma_2, \tag{47}$$

$$\mathcal{H}_{K'} = -\mathcal{H}_K, \tag{48}$$

where M is proportional to $\epsilon_A - \epsilon_B$.

Again, we first consider the edge states for the PEC/PMC boundary. Figure 7 shows the photonic band structure of the edge states with the PEC or PMC boundary.

[Figure 7 about here.]

In all the cases, the edge states are gapped. However, it is remarkable that, as for the zigzag edge, the upper edge states of the PEC boundary and the lower edge states of the PMC boundary are nearly gapless. Moreover, these dispersions are almost linear around the K and K' valleys.

These properties are fully understood by the effective hamiltonian. Following a similar argument as we did in Sec. 3, we can easily find that the results are consistent with the effective hamiltonian with $v > 0$ and $M < 0$. More intuitively, the following argument also explain the properties. The PEC or PMC wall is like a mirror and the mirror-inverted image of the PhC is the PhC with swapped A and B sites. Therefore, the system with the PEC/PMC wall imitates a combined system with a domain wall. As in the domain-wall fermion, the edge states becomes linear and nearly gapless around the K and K' valleys. In the other cases of the upper edge states of the PMC boundary and the lower edge states of the PEC boundary are almost absent. In these cases, although the domain wall is formed, their masses have the same sign between the two domain, so that the edge states are almost absent. As for the armchair edge, the edge states are clearly gapped regardless of either the PEC or PMC boundary. By symmetry, the upper- and lower-edge states are completely degenerate.

Next, we consider the open boundary. The dispersion relation of the edge states are shown in Fig. 8.

[Figure 8 about here.]

Again, the edge states are clearly gapped. As for the armchair edge, the upper- and lower-edge states are completely degenerate. By increasing the distance between the PEC wall and PhC edge, we can see a smooth transition of the edge states to those in the open boundary, while keeping the gapped property.

In this way, the edge states of the nontopological PhC are gapped irrespective of the boundary conditions., supporting the bulk-edge correspondence.

5. Summary

In summary, we have presented a detailed theoretical analysis on topological and nontopological PhCs with open boundary. The openness of the system is caused by intrinsic properties of photons and yields imaginary parts in the eigenfrequency spectrum of edge states. The transfer-matrix formalism and resulting semi-infinite reflection matrices together with the Krein-Friedel-LLoyd formula of the DOS enable us to determine the leaky and guided edge-state dispersion relations accurately. The leaky edge states inside the light cone emerge as Lorentzian peaks of the DOS spectrum, whose peak and width in frequency correspond to the eigenfrequency and inverse quality factor of the edge state. Taking the width into account, the edge-state dispersion is shown to be chiral and gapless for topological PhCs with nonzero Chern numbers. The edge states for nontopological PhCs with vanishing Chern number are shown to be gapped. In this sense, the bulk-edge correspondence certainly holds even for the open photonic systems.

Acknowledgements

This work was partially supported by KAKENHI Grant No. 17K05507.

References

[1] Haldane FDM, Raghu S. Possible Realization of Directional Optical Waveguides in Photonic Crystals with Broken Time-Reversal Symmetry. Phys Rev Lett. 2008;100(1):013904.

[2] Ozawa T, Price HM, Amo A, et al. Topological photonics. Rev Mod Phys. 2019 Mar; 91:015006.

[3] Hatsugai Y. Chern number and edge states in the integer quantum Hall effect. Phys Rev Lett. 1993;71(22):3697–3700.

[4] Ochiai T, Onoda M. Photonic analog of graphene model and its extension: Dirac cone, symmetry, and edge states. Phys Rev B. 2009;80(15):155103.

[5] Botten LC, Nicorovici NA, McPhedran RC, et al. Photonic band structure calculations using scattering matrices. Phys Rev E. 2001;64(4):046603.

[6] Li ZY, Ho KM. Light propagation in semi-infinite photonic crystals and related waveguide structures. Phys Rev B. 2003 Oct;68:155101.

[7] Krein M. Matem Sbornik. 1953;33:597.

[8] Friedel J. Nuovo Cimento Suppl. 1958;7:287.

[9] Lloyd P. Pseudo-potential models in the theory of band structure. Proc Phys Soc London. 1965 oct;86(4):825–832.

[10] Hatano N, Nelson DR. Localization transitions in non-hermitian quantum mechanics. Phys Rev Lett. 1996 Jul;77:570–573.

[11] Bender CM, Boettcher S. Real spectra in non-hermitian hamiltonians having PT symmetry. Phys Rev Lett. 1998 Jun;80:5243–5246.

[12] Breuer HP, Petruccione F, et al. The theory of open quantum systems. Oxford University Press on Demand; 2002.

[13] Gong Z, Ashida Y, Kawabata K, et al. Topological phases of non-hermitian systems. Phys Rev X. 2018 Sep;8:031079.

[14] Yao S, Wang Z. Edge states and topological invariants of non-hermitian systems. Phys Rev Lett. 2018 Aug;121:086803.

[15] Yoshida T, Peters R, Kawakami N. Non-hermitian perspective of the band structure in heavy-fermion systems. Phys Rev B. 2018 Jul;98:035141.

[16] Ohtaka K, Numata H. Multiple-scattering effects in photon diffraction for an array of cylindrical dielectrics. Phys Lett A. 1979;73(5-6):411–413.

[17] Ohtaka K, Ueta T, Amemiya K. Calculation of photonic bands using vector cylindrical waves and reflectivity of light for an array of dielectric rods. Phys Rev B. 1998;57(4):2550–2568.

[18] Leung KM, Qiu Y. Computation of complex band structures and transmission spectra of 2-d photonic crystals using a layer-kkr method. Electromagnetics. 1999;19(3):305–319.

[19] Pendry JB. Low energy electron diffraction. London: Academic; 1974.

[20] Faulkner J. Scattering theory and cluster calculations. J Phys C: Solid State Phys. 1977; 10(23):4661.

[21] Ohtaka K, Inoue J, Yamaguti S. Derivation of the density of states of leaky photonic bands. Phys Rev B. 2004;70(3):035109.

[22] Jackiw R, Rebbi C. Solitons with fermion number 1/2. Phys Rev D. 1976;13:3398–3409.

[23] Ochiai T. Broken symmetry and topology in photonic analog of graphene. Int J Mod Phys B. 2014;28(02):1441004.

[24] Ochiai T. Photonic realization of the (2+1)-dimensional parity anomaly. Phys Rev B. 2012;86:075152.

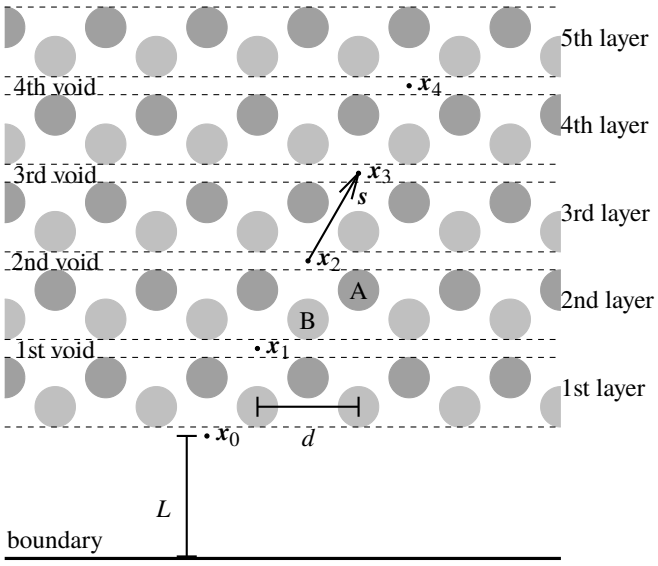

Figure 1. Schematic illustration of the honeycomb-lattice photonic crystal presented in this paper. It consists of a periodic stack of identical monolayers with relative shift $\boldsymbol{s}$. The monolayer is a periodic arrangement of circular cylinders with period d in the x direction.

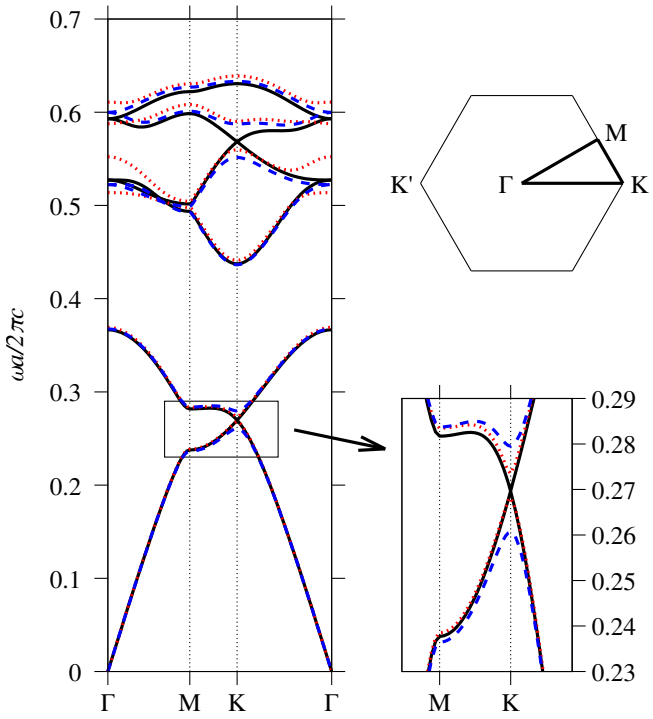

Figure 2. Bulk photonic band structures of the honeycomb-lattice PhCs made of circular rods. The rods have dielectric constant $\epsilon_{\mathrm{A(B)}}$, diagonal permeability $\mu_{\mathrm{A(B)}}$, imaginary off-diagonal permeability $\kappa_{\mathrm{A(B)}}$, and radius $r_{\mathrm{A(B)}}$ for the A(B) sites of the honeycomb lattice. The background medium is air ($\epsilon = \mu = 1, \kappa = 0$). Three configurations are considered: 1) $\epsilon_{\mathrm{A}} = \epsilon_{\mathrm{B}} = 12$ and $\kappa_{\mathrm{A}} = \kappa_{\mathrm{B}} = 0$ (solid line), 2) $\epsilon_{\mathrm{A}} = \epsilon_{\mathrm{B}} = 12$ and $\kappa_{\mathrm{A}} = \kappa_{\mathrm{B}} = 0.2$ (dotted line), and 3) $\epsilon_{\mathrm{A}} = 13, \epsilon_{\mathrm{B}} = 11$ and $\kappa_{\mathrm{A}} = \kappa_{\mathrm{B}} = 0$ (dashed line). The other parameters are kept fixed as $\mu_{\mathrm{A}} = \mu_{\mathrm{B}} = 1$ and $r_{\mathrm{A}} = r_{\mathrm{B}} = 0.2a$, where a is the lattice constant of the honeycomb lattice. The upper right inset shows the first Brillouin zone of the honeycomb lattice. Points of high symmetry are noted.

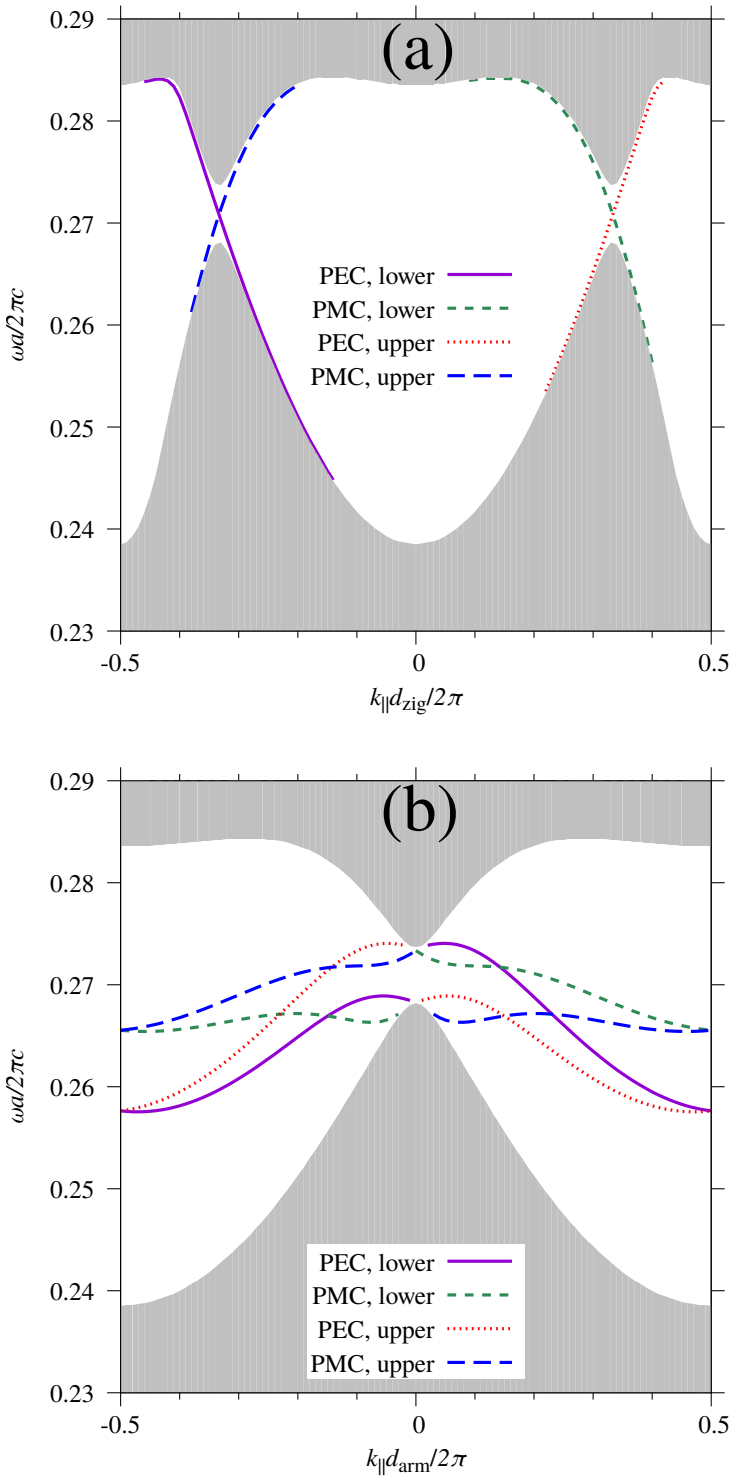

Figure 3. Photonic band structures of (a) the zigzag and (b) armchair edge states for the PEC or PMC boundary. The following PhC parameters are assumed: $\epsilon_A = \epsilon_B = 12$, $\mu_A = \mu_B = 1$, $\kappa_A = \kappa_B = 0.2$, and $r_A = r_B = 0.2a$. The shaded region represents the bulk photonic bands and the blank region is the photonic band gap. We consider the upper and lower edges of the semi-infinite PhC in the perpendicular direction to the edge. The symbol $d_{\mathrm{zig(arm)}}$ represents the spatial periodicity in the zigzag (armchair) edge and is given by $d_{\mathrm{zig}} = a$ and $d_{\mathrm{arm}} = \sqrt{3}a$. The distance L to the PEC/PMC boundary (See Fig. 1) is taken to be zero, assuming the reference point $\boldsymbol{x}_n$ on the mirror plane for the zigzag edge, and a glide planes for the armchair edge.

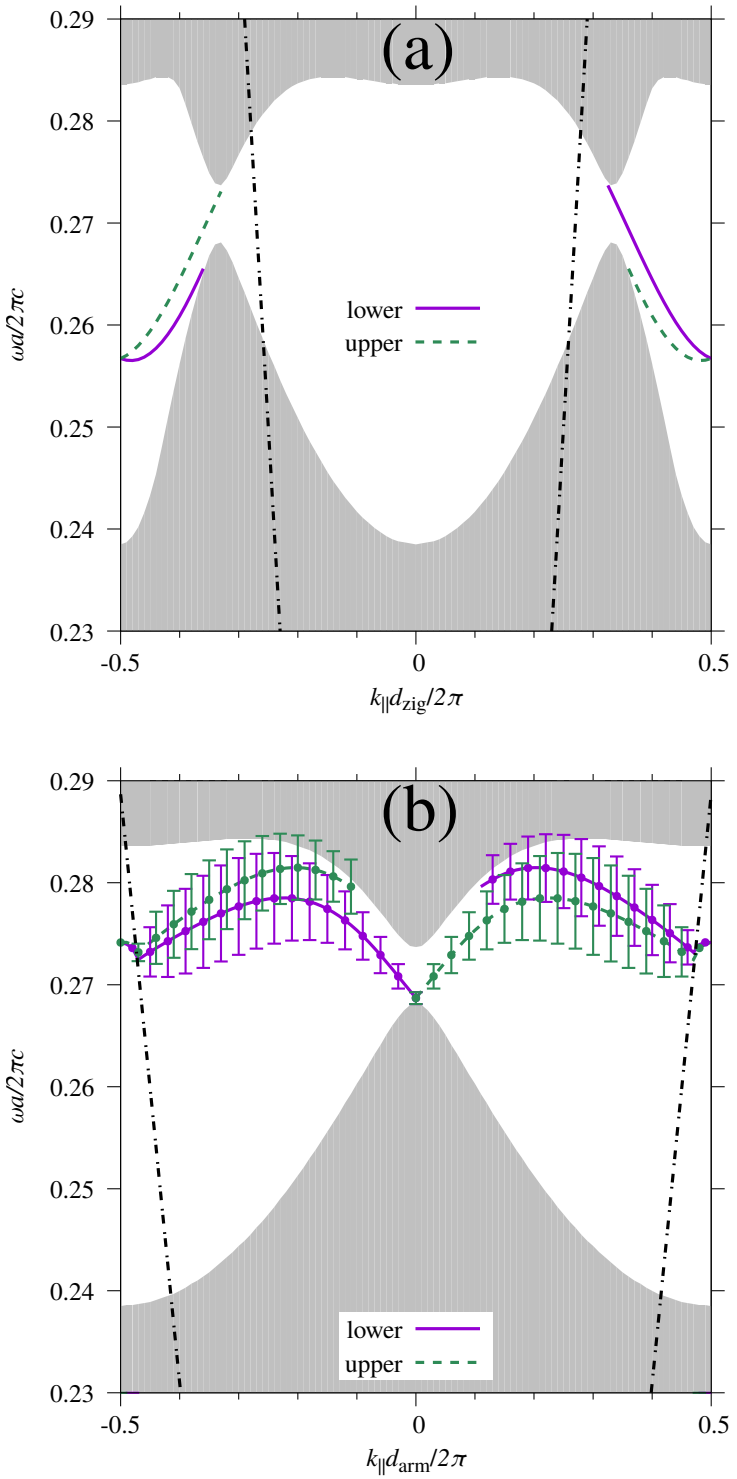

Figure 4. Photonic band structures of (a) the zigzag and (b) armchair edge states for the open boundary. Both the upper and lower edges of the semi-infinite PhC are considered. The PhC parameters are the same as in Fig. 3. The dash-dotted line is the light cone $\omega = c|k_{\|}|$. Inside the light cone $\omega > c|k_{\|}|$, the edge states become leaky having finite lifetimes. The error bar length represents the inverse lifetime Γ of the edge states.

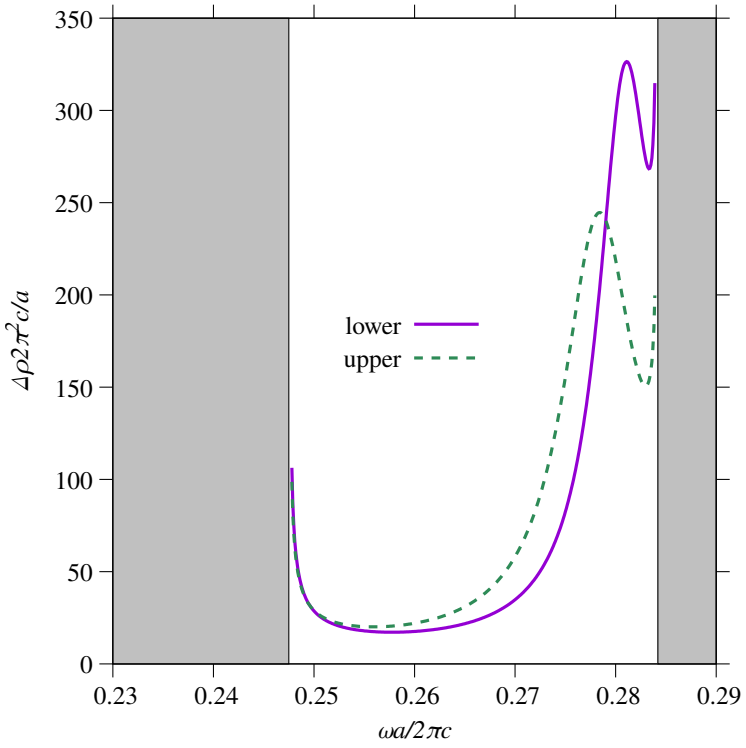

Figure 5. Increment of the optical density of states $\Delta\rho$ due to the presence of the semi-infinite PhC with the open armchair edge. Both the upper and lower edges are considered. The PhC parameters are the same as in Fig. 3. The momentum parallel to the boundary is taken to be $k_{\|} d_{\mathrm{arm}}/2\pi = 0.25$.

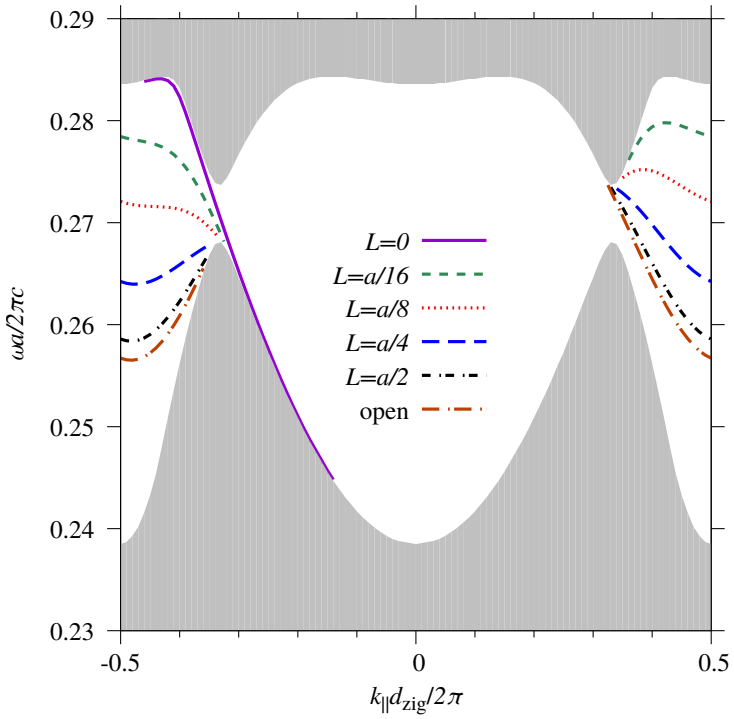

Figure 6. Dependence of the edge-state dispersion on the distance L from the PhC edge to the PEC wall. The lower zigzag edge is considered. The PhC parameters are the same as in Fig. 3.

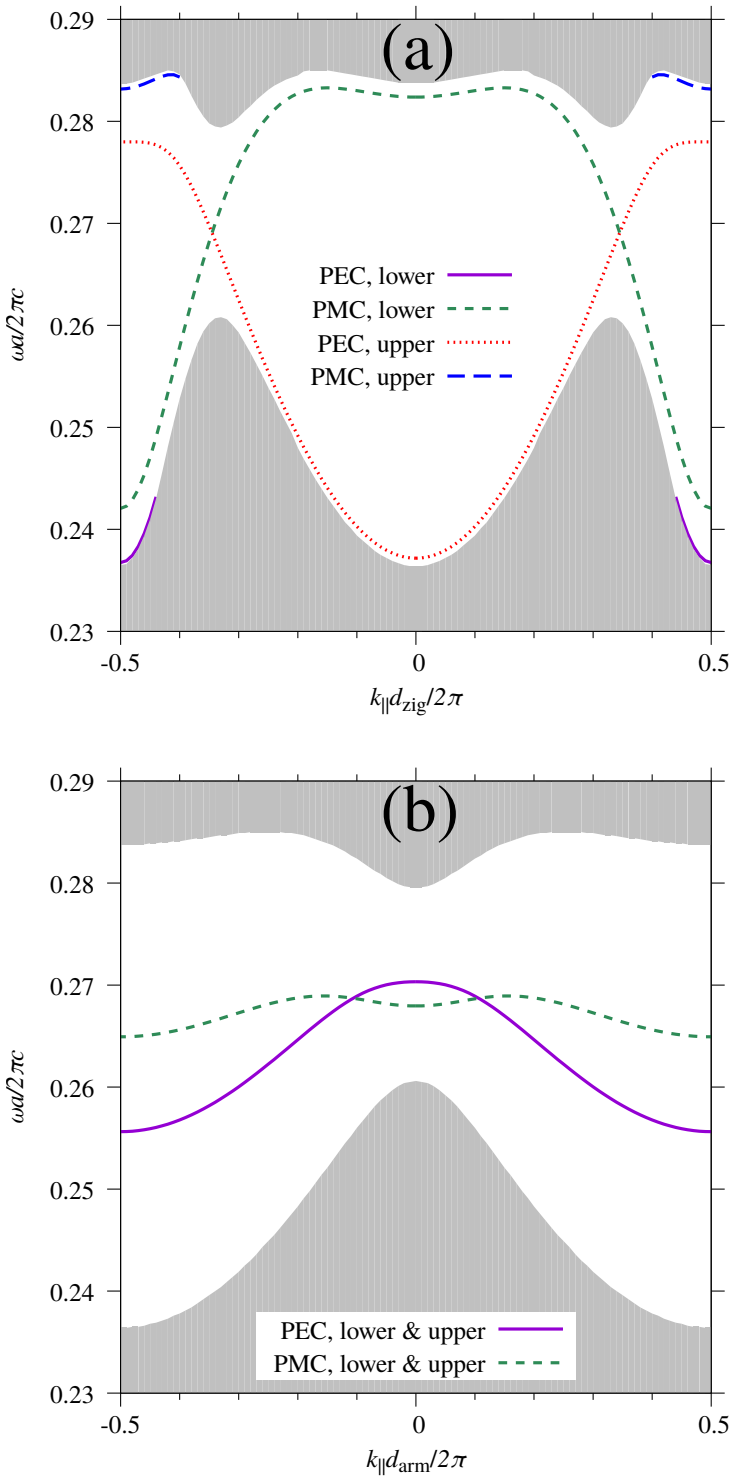

Figure 7. Photonic band structures of (a) the zigzag and (b) armchair edge states in the honeycomb lattice PhC with the time-reversal symmetry but without the space-inversion symmetry. The PhC parameters are as follows: $\epsilon_A = 13$, $\epsilon_B = 11$, $\mu_A = \mu_B = 1$, $\kappa_A = \kappa_B = 0$, and $r_A = r_B = 0.2a$. Both the upper and lower edges of the semi-infinite PhC are considered. In the armchair case, the upper and lower edge states are completely degenerate by symmetry. The boundary is capped by the PEC/PMC wall with distance $L = 0$.

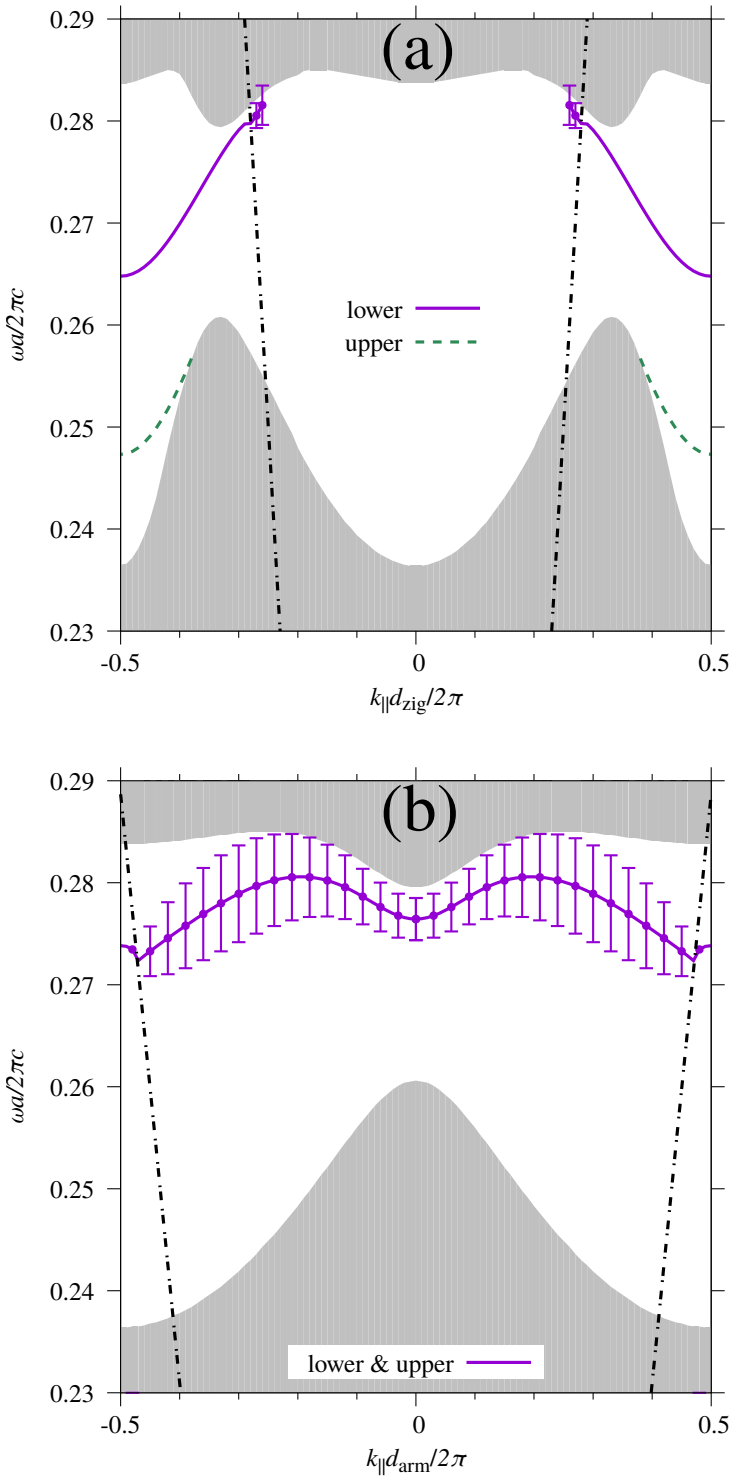

Figure 8. Photonic band structures of the edge states in the honeycomb lattice PhC with the time-reversal symmetry but without the space-inversion symmetry. The PhC parameters are the same as in Fig. 7. The boundary is open to air. The dash-dotted line is the light cone $\omega = c|k_{\parallel}|$. The error bar length represents the inverse lifetime Γ of the edge states.